Quaternary Science Reviews 246 (2020) 106533

Contents lists available at ScienceDirect

Quaternary Science Reviews

journal homepage: www.elsevier.com/locate/quascirev

Invited paper

Late Holocene dynamics of the south American summer monsoon: New insights from the Andes of northern Chile (21°S)

Ignacio A. Jara [a, *], Antonio Maldonado [a, b, c], María Eugenia de Porras [d]

[a] Centro de Estudios Avanzados en Zonas Áridas (CEAZA), Raúl Bitrán 1305, La Serena, Chile
[b] Instituto de Investigación Multidisciplinario en Ciencia y Tecnología, Universidad de La Serena, Raúl Bitrán 1305, La Serena, Chile
[c] Departamento de Biología Marina, Universidad Católica del Norte, Larrondo, 1281, Coquimbo, Chile
[d] Instituto Argentino de Nivología, Glaciología y Ciencias Ambientales (IANIGLA) – CCT Mendoza CONICET. Av. Ruiz Leal s/n, Mendoza, Argentina

ARTICLE INFO

Article history:
Received 29 May 2020
Received in revised form
4 August 2020
Accepted 5 August 2020
Available online xxx

ABSTRACT

The South American summer monsoon (SASM) is the most important climate system of tropical South America, transporting moisture from the tropical Atlantic Ocean to the core of the continent during the austral summer. Recent paleoclimate studies suggest that past variability of the SASM has been more heterogenous in space and time than previously thought, implying that different atmospheric drivers controlled its long-term evolution. Unfortunately, past SASM reconstructions are largely limited to the last 2000 years and mainly focused on the core of the monsoon domain where precipitation does not fall exclusively during the monsoon season, thereby limiting our understanding of its long-term changes, drivers and mechanisms. Here we present a new 4000-year SASM precipitation reconstruction based on a high-resolution pollen sequence from a mountain lake in the dry Andes of northern Chile (21°S). We provide evidence for two centennial-scale intervals of enhanced SASM precipitation between 4000–3400 and 2300-1900 cal yr BP. These intervals are replicated in records from the southern portion of the central Andes (>18°S) but not clearly detected further north, suggesting the existence of a monsoon dynamics largely decoupled from latitudinal shifts of the Intertropical Convergence Zone. A comparison with precipitation reconstructions from the entire SASM domain and modern climate datasets suggests a teleconnection with the Southern Hemisphere circulation through the intensification of the South Atlantic Convergence Zone and/or the intrusion of extra-tropical Atlantic moisture. Our results highlight that significant spatial and temporal variability of the SASM occurred during the most recent millennia, and therefore social and environmental forecast should consider that similar variations will likely occur in the future.

1. Introduction

The South American summer monsoon (SASM) is a critical climate feature for tropical and subtropical regions of South America. Monsoon-derived hydrological resources represent an important environmental commodity for the socio-economic activities of more than 60% of South American population (Pascale et al., 2019). Observational measurements of the SASM over the last two decades have revealed significant variations of its year-to-year strength (De Carvalho and Jones, 2015), which have resulted in the occurrence of extreme events such as drought or floods in many parts of South America (Boers et al., 2016; Erfanian et al., 2017; Grimm, 2019; Sulca et al., 2018). Yet, whether or not the modern ranges of monsoon variability will characterize its future behaviour is still largely unknown (Neukom et al., 2015). Constraining future uncertainties requires a better understanding of the SASM variability at different temporal and spatial levels. Paleoclimate studies are able to improve this understanding by reconstructing monsoon responses at time-scales that exceed modern ranges of variation, permitting a more complete assessment of local and remote drivers and mechanisms.

A significant number of SASM reconstructions from the tropical Andes (5–13°S; 70–77°W) and eastern Brazil (10–14°S; 39–43°W) (Fig. 1a), two regions in the core of the SASM domain, have shown considerably variability during the Holocene at scales ranging from decadal to multi-millennial (Bird et al., 2011a; Bustamante et al.,

* Corresponding author.
E-mail address: ignacio.jara@ceaza.cl (I.A. Jara).

https://doi.org/10.1016/j.quascirev.2020.106533
0277-3791/

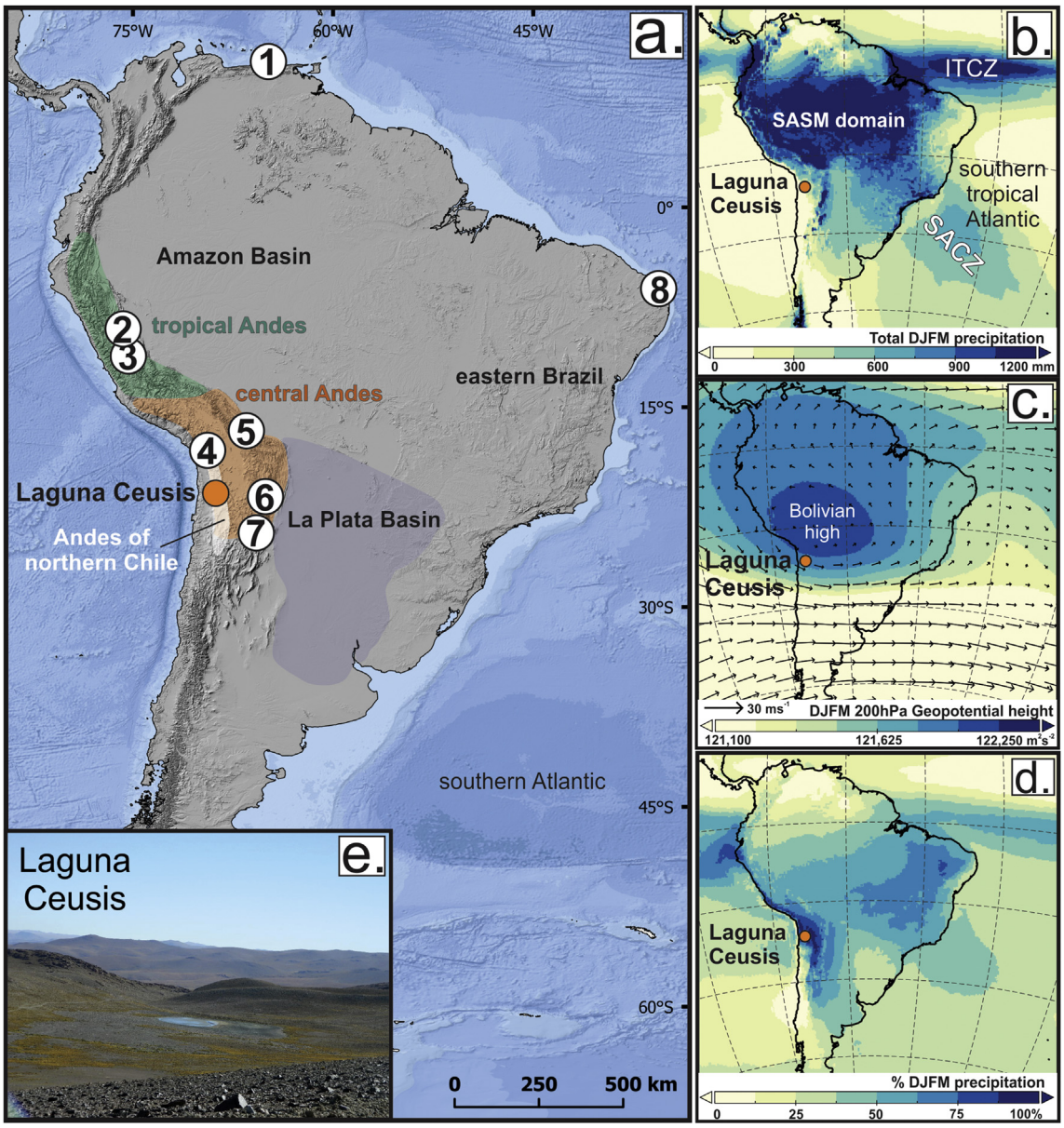

Fig. 1. Geographic and climatic settings of the study area and study site. (a) General physiographic aspects of South America with the location of main geographic units and records mentioned in the main text: (1) Cariaco Basin (Haug et al., 2001), (2) Laguna Pumacocha (Bird et al., 2011a), (3) Huagapo Cave (Kanner et al., 2013), (4) Lago Chungará (Jara et al., 2019), (5) Umajalanta–Chiflonkhakha cave system (Apaéstegui et al., 2018), (6) Santa Victoria peat mire (Hooper et al., 2020), (7) Cerro Tuzgle (Kock et al., 2019) and (8) Boqueirão Lake (Utida et al., 2019). (b) South American summer monsoon (SASM) region defined as total summer (DJFM) precipitation, ITCZ =Inter Tropical Convergence Zone, SACZ = South Atlantic Convergence Zone. (c) The Bolivian high pressure cell defined by 200 hPa wind vectors (scale at bottom) and geopotential height. (d) Percentage of summer precipitation. (e) Laguna Ceusis (LC) and surrounding slopes. Photo credits to María Eugenia de Porras. All atmospheric data corresponds to mean (1980–2019) values of ERA5 reanalysis total precipitation at the surface (10 m), and geopotential height and eastward/northward wind components at the upper-troposphere (12,000 m) level. All data is freely provided by the European Centre for Medium-Range Weather Forecasts (ECMWF).

2016; Cheng et al., 2009). The last 2000 years is by far the best documented period, with the Medieval Climate Anomaly (MCA; 1050-850 cal yr BP) and the Little Ice Age (LIA; 450-100 cal yr BP) the best documented centennial-scale events (Bird et al., 2011b; Vuille et al., 2012). Past SASM anomalies inferred from oxygen isotopes ($\delta^{18}O$) excursions in sedimentary archives such as speleothems, lakes and ice cores indicate that a reduction of SASM precipitation occurred during the MCA, while a relatively strengthening of monsoonal activity was experienced during the LIA (Bird et al., 2011b; Vuille et al., 2012). Close correspondence between reconstructions from the core of the SASM domain, records from the tropical Atlantic, and Northern Hemisphere temperature reconstructions provide strong support that latitudinal shifts in the Intertropical Convergence Zone (ITCZ) -ultimately driven by temperature variability in the north Atlantic-have been a major forcing of SASM precipitation trends during the MCA and LIA (Campos et al., 2019; Haug et al., 2001; Putnam and Broecker, 2017; Vuille et al., 2012). The notion that these climate events represented significant anomalies in the context of the Holocene has been backed by records from the entire domain of SASM influence (Bird et al., 2011b; Campos et al., 2019), by the fact that a regionally-coherent cooling signal is observed in tropical South America between 350 and 150 cal yr BP (Neukom et al., 2019), and by documented Andean glaciers advances (Jomelli

et al., 2011; Rabatel et al., 2013). However, other reconstructions reveals that the LIA and MCA may not represent the only significant centennial-scale anomalies during the Holocene. For instance, $\delta^{18}O$ variations in records from the tropical Andes show considerable precipitation excursions that predate the occurrence of LIA and the MCA (Kanner et al., 2013; Seltzer et al., 2000; Van Breukelen et al., 2008); whereas isotopic and lake level variations in northeastern Brazil reveal large shifts in precipitation between 2500 and 650 cal yr BP (Utida et al., 2019; Viana et al., 2014). Documenting centennial-scale precipitation anomalies prior to the MCA and LIA is needed to assess if the drivers and mechanisms that dominated the most recent millennia of monsoonal variability did also operate in previous Holocene periods.

The identification of Holocene SASM anomalies have gained further relevance with a series of recent paleoclimatic reconstructions from the central Andes (14–24°S; 75-65°W; Fig. 1a), on the southwestern margins of the SASM domain, showing considerable spatial heterogeneities in relationship with records from the core of the SASM region (Apaéstegui et al., 2018; Jara et al., 2019; Kock et al., 2020). These differences have been explained in the light of interactions between tropical and extra-tropical drivers, as well as the contribution of different moisture sources (Kock et al., 2020; Novello et al., 2016; Stríkis et al., 2011). For instance, differences between the tropical and central Andes regions are consistent with the south Atlantic Ocean as an additional moisture source for the monsoon in its southern domain. (Apaéstegui et al., 2018). Similarly, Jara et al. (2019) showed that, unlike the tropical Andean region, past precipitation variability in the central Andes was largely decoupled from changes in the ITCZ and the tropical Pacific Ocean. Despite this new evidence, the identification of centennial-scale SASM anomalies and their expression across the entire SASM domain has been hampered by the fact that: (1) well-dated, high-resolution records are mainly limited to the last 2000 years, and (2) monsoon reconstructions are concentrated in the core of the SASM domain where rainfall is relatively well distributed through the year, and therefore precipitation reconstructions are not exclusively linked to monsoonal variability.

To improve our understanding of Holocene SASM changes, we present a new precipitation reconstruction based on a high-resolution pollen analysis from a lake core that extends continuously for the last 4000 years in the dry Andes of northern Chile (21°S). This region corresponds to the southwestern tail of the SASM region, being the only area in South America in which precipitation occurs almost exclusively during the monsoon season. Past precipitation trends are reconstructed from relative changes in terrestrial vegetation, sediment accumulation rates and lake level inferences. We discuss such trends in the context of other reconstructions from the entire region of SASM influence in order to assess the temporal and spatial variability of the SASM during the most recent millennia. We further explore this variability in the light of modern climatological studies to propose potential sources and mechanisms of past monsoon change.

2. Regional setting

2.1. Climate

Originating from the seasonal variation of the continental-ocean thermal contrast, the SASM is the most important circulation feature of tropical and subtropical South America (Baker and Fritz, 2015; Zhou and Lau, 1998). Between December and March, the continental-ocean thermal gradient deepens and the easterly trade winds embedded in the ITCZ are pushed southwards to the continental interior, transporting moisture of tropical Atlantic origin across the Amazon Basin and the tropical and central Andes through a northerly flow of convective precipitation (Garreaud et al., 2009; Viveen et al., 2019, Fig. 1b). At the peak of the monsoon season, a northwest-southeast band of convection is also formed (the South Atlantic Convergence Zone, SACZ), connecting the core of the monsoon region with the southwestern Atlantic Ocean (Rosa et al., 2020, Fig. 1b). Upper-level (< 500 hPa) circulation exerts a major role controlling the strength and spatial extension of the monsoon (Lenters and Cook, 1999). During a strong SASM, an intensification and southward migration of the upper-atmosphere anticyclonic circulation -the Bolivian high- promotes a more vigorous upper-level easterly flow, leading to enhanced movement of moist air masses at the surface and heightening convective activity (Fig. 1c). Conversely, during a weak monsoon development the upper-atmosphere circulation is weakened and the easterly winds reduced, giving way to a drier westerly wind anomaly and thereby less continental precipitation (Lenters and Cook, 1997; Vuille and Keimig, 2004).

Inter-annual variability of monsoon precipitation arises from large-scale teleconnections with different circulation systems. The occurrence of El Niño or La Niña events (ENSO) in the tropical Pacific Ocean is an important source of year-to-year variability as ENSO-related rainfall anomalies in South America tend to occur during austral summer along with the monsoon season. The influence of ENSO on SASM precipitation operates through the mechanisms of monsoon variability mentioned in the previous paragraph, leading to enhanced (reduced) SASM precipitation during La Niña (El Niño) years (Sulca et al., 2018). In addition, ENSO-like variability in austral summer precipitation is also observed at decadal timescales in association with the Pacific Decadal Oscillation (Garreaud et al., 2009; Segura et al., 2016). By controlling the latitudinal position of the ITCZ, tropical and north Atlantic sea surface temperatures also exert an important control in the SASM strength from interannual to centennial timescales (Canedo-Rosso et al., 2019; Nobre and Shukla, 1996). In general, warming (cooling) in the north Atlantic Ocean results in a northward (southward) migration of the ITCZ and overall reduced (increased) SASM intensity (Han et al., 2019).

The central Andean mountains correspond to the southwestern margins of the SASM domain (Fig. 1a). At its widest, the central Andes is dissected into a western and an eastern cordillera, separated by the width of the high-elevation plateau or *Altiplano*. Strong rainfall gradients in precipitation are locally determined by the rugged mountainous topography, and regionally by the intersection of the low-level moisture flow with the Andes massif. As a result, the southern and western portions of the central Andes are significantly drier than the northern and eastern sides (Vuille, 1999). The southwestern flanks of the central Andes corresponds to the Andes of northern Chile (17°S to 26°S; Fig. 1a). This region represents the southwestern tail of the SASM domain, and therefore monsoon precipitation is scarce (20–500 mm yr^{-1}). Although rain and snowfall events of Pacific origin occur as a result of occasional cold fronts or cut-off low pressure waves during austral winter months (Reyers and Shao, 2019; Vuille and Ammann, 1997), precipitation in the Andes of northern Chile is heavily concentrated during the summer (>75% Viale et al., 2019, Fig. 1d). It is therefore not surprising that variations in the monsoon intensity from interannual to decadal timescales have produced a significant impact on regional precipitation (Aceituno and Montecinos, 1993; Vuille and Keimig, 2004).

2.2. Vegetation

The vegetation of the central Andes is extremely rich and diverse, ranging from humid montane forest on the eastern cordillera, to high-Andean steppe in the Altiplano, to xerophytic

shrubland on the drier western slopes (Brush, 1982). Large-scale vegetation patterns mimic the strong temperature and moisture gradients established by the rugged Andean topography and the northeasterly source of precipitation, and therefore shifts in plant distribution during the late Quaternary have largely been driven by precipitation changes (Baker and Fritz, 2015). On the dry western Andes slopes of northern Chile, vegetation composition, structure and richness exhibit marked altitudinal transformations from the unvegetated planes of the Atacama Desert up to the Andean steppe and forest ecosystems (Collao-Alvarado et al., 2015; Villagrán et al., 1981, 1983). Modern vegetation and pollen transects in this arid environment show the establishment of distinct altitudinal vegetation zones or belts (de Porras et al., 2017; Jara et al., 2019; Latorre et al., 2003; Maldonado et al., 2005). These published transects have also revealed that the floristic and palynological composition of these belts reflect the close relationship between summer precipitation and elevation in the western slopes of the Andes of northern Chile, and therefore past precipitation inferences can be drawn from changes in vegetation distribution. In the following paragraphs we provide a description of the main floristic elements of the Andes of northern Chile, based on the scheme proposed by Collao-Alvarado et al. (2015), further complemented by additional vegetation surveys (Teillier, 2004; Trivelli and Valdivia, 2009), and following the taxonomic nomenclature presented by Rodríguez et al. (2018).

At about 21°S the inland penetration of the hyperarid core of the Atacama Desert extends up to 2600 masl, delineating the lower limit of vegetation. Above that, annual precipitation up to 50 mm year^{-1} allows the establishment of a low-density (plant coverage <15%) arrangement of xerophytic perennial shrubs referred as Prepuna belt. This community is largely dominated by the shrub *Atriplex imbricata* (Amaranthaceae), along with other perennial taxa such as *Baccharis boliviensis* (Asteraceae), *Fabiana densa* (Solanaceae), *Aloysia deserticola* (Verbenaceae), *Cistanthe salsoloides* (Montiaceae), *Adesmia rahmeri* (Fabaceae) and the gymnosperm *Ephedra americana* (Ephedraceae). Annuals and perennial herbs such as *Tiquilia atacamensis* (Boraginaceae), *Mostacillastrum* spp., (Brassicaceae), *Lepidium* spp. (Brassicaceae), *Hoffmannseggia doellii* (Fabaceae), and Cactaceae species from the *Maihueniopsis* genus such as *M. camachoi* and *M. glomerata*, along with *Tunilla soehrensii* are also present.

Above 3200 masl, the Prepuna belt is progressively replaced by a more diverse and densely assorted community of perennial shrubs (plant cover 20–30%). This vegetation community, called Puna belt, develops in areas where precipitation ranges between 70 and 150 mm yr^{-1} and supports perennial shrubs such as *Fabiana densa*, *Baccharis boliviensis*, *B. tola*, *Parastrephia quadrangularis* (Asteraceae), *P. teretiuscula*, *Chuquiraga atacamensis* (Asteraceae), *Mutisia hamata* (Asteraceae), *Fabiana denudata*, *F. ramulosa*, *Senecio viridis* (Asteraceae), *Adesmia hystrix*, *Lampayo medicinalis* (Verbenaceae) and *E. americana*. These perennial shrubs are accompanied by a significant number of summer annuals such as *Junellia seriphioides* (Verbenaceae), *Cryptantha* spp. (Boraginaceae), *Laennecia artemisioides* (Asteraceae), *Tagetes multiflora* (Asteraceae) among several others; and the Cacti *Cumulopuntia ignescens* and *Maihueniopsis glomerata*. In the upper limit of this belt, tussock grasses such as *Jarava pogonathera* (Poaceae) and *Festuca chrysophylla* (Poaceae) intermixed with the aforementioned shrubs species.

High-Andean steppe replaces Puna shrubland at around 3800–4000 masl where mean annual precipitation is above 150 mm yr^{-1}. This vegetation belt is essentially dominated by *Festuca chrysophylla* and other tussock grasses of the Poaceae family such as *Deschampsia caespitosa*, *Nassella nardoides*, *Pappostipa frigida*, *Anatherostipa venusta* and *Festuca arundinacea*. Some species of the Puna belt extend their distribution into the high-Andean steppe, including *P. quadrangularis*, *Senecio nutans*, *S. volckmannii*, *Junellia pappigera*, *J. digitata*, *Adesmia subterranea*, *Trichocline deserticola* (Asteraceae). On rocky substrates above 4000 masl, the cushion shrub *Azorella compacta* (Apiaceae) is the main floristic element of the Subnival belt, a formation characterized by scattered herbaceous plants, dwarf shrubs, mosses and lichens that extends up to the snow line. *A. compacta* is indeed one of the woody plants occurring at higher elevation in the world, reaching up to 5200 masl in the Andes of northern Chile (Pugnaire et al., 2020). Vascular plants characteristic of the Subnival belt are *P. quadrangularis*, *B. tola*, *L. medicinalis*, *Pycnophyllum bryoides* (Caryophyllaceae), *P. macropetalum*, *Perezia atacamensis* (Asteraceae) and *Azorella atacamensis*. Gorges and valley bottoms between 4200 and 5000 masl are sometimes occupied by woodlands of *Polylepis tarapacana* (Rosaceae) along with *P. quadrangularis*, *B. tola*, *Fabiana squamata*, *M. camachoi*, and several other Puna perennial shrubs.

2.3. Study site

Laguna Ceusis (21.04 °S, 68.66 °W; Fig. 1e) is a small (0.01 km^2), high elevation (4670 masl), shallow (<1 m) lake located in the dry Andes of northern Chile, on the southwestern margins of the central Andes. Laguna Ceusis (LC) is a closed basin of approximately 105 m long and 78 m wide and, as such, water gets into the lake directly from rainfall and/or from surface runoff of the surroundings slopes. The lake is located ~8 km south from the *Doña Inés de Collahuasi* mining complex, at the bottom of small gorge amidst a mountainous area composed of Carboniferous-Permian granites (SERNAGEOMIN, Chile). This mountainous area emerges from a basement covered by Tertiary ignimbrites and volcanic rocks, forming the Andean headwaters of the Río Loa, the only river able to reach the Pacific coast in the Atacama region (McKee, 2001). To the east, a complex of more than ten Tertiary-to-Quaternary eruptive domes results in a landscape marked by volcanic and hydrothermal deposits. Mean annual precipitation around LC ranges from 40 to 480 mm yr^{-1} (average 1970–2018 = 160 mm yr^{-1}), with 88% of the annual amount falling during the monsoon season, between December and March (data freely available from the Explorador Climatico, CR2). Mean annual temperature is 3.6 °C, rising up to 7.6 °C during the warmest month (February) and dropping to −1 °C during the coldest (August). As a result, the climate around LC is cold and semi-arid with a marked summer rainy season. Precipitation is concentrated during summer months (Fig. 1d), and therefore it becomes an ideal site to investigate past variations in SASM precipitation. This is in stark contrasts with most of other tropical and subtropical regions of South America where around 40–70% of annual precipitation falls during the austral summer (Rosa et al., 2020, Fig. 1d). Common plants in the LC catchment area include *F. chrysophylla*, *Fabiana squamata*, *B. tola*, *P. tarapacana, P. bryoides*, *N. nardoides*, *P. frigida*, *Festuca hypsophyla* and *P. quadrangularis*.

3. Material and methods

3.1. Stratigraphy and chronology

Two overlapping short cores were collected in 2015 from an inflatable boat anchored at the deepest part of LC using an UWITEC gravity coring system. Both cores were subsequently stored in a cold room (4 °C) protected by their respective PVC liners at the Laboratory of Paleoecology and Paleoclimate at the Centro de Estudios Avanzados en Zonas Áridas (CEAZA), Chile. Once cut in halves, the stratigraphy of short core number two (SHC-2; 43.5-cm-long) was visually characterized and further analysed with the aid

of a Loss On Ignition (LOI) analysis. LOI analysis followed standard procedures including combustions at 105 °C (overnight), 550 °C (4 h) and 925 °C (12 h) to quantify the water, organic matter and carbonate content respectively (Heiri et al., 2001). In the absence of macroscopic remains from terrestrial plants, the chronology of core SHC-2 was constrained by AMS radiocarbon dating performed on bulk sediments. Dating of the upper-most centimetre allowed the assessment of potential reservoir effect. Calibration of radiocarbon ages was conducted using the Southern Hemisphere calibration curve SHCAL13 (Hogg et al., 2013). All calibrated ages were incorporated into a Bayesian age-depth model using the Bacon packages in the R-studio platform (Blaauw and Christen, 2011; R Core Team, 2014). Age-depth modelling was performed with a total of 23 sections (section thickness = 2 cm), with a maximum depth of 45 cm. Prior information included a mean sediment accumulation of 100 yr cm^{-1}, an accumulation shape of 1.5 yr cm^{-1}, a memory mean of 0.7 and a memory strength of 4. The age-depth model allowed the estimation of the Sediment Accumulation Rate (SAR; cm yr^{-1}) which, due to the absence of inlets to the lake, is assumed to result from endogenous organic productivity and/or precipitation-driven surface runoff from the lake catchment area (Matthias and Giesecke, 2014).

3.2. Pollen analysis

A total 86 samples were taken at contiguous 0.5 cm intervals along the entire length of core SHC-2. Pollen processing followed standard procedures, including KOH deflocculation, HCL and HF treatments to dissolve carbonates and siliciclastic material, acetolysis reaction to remove cellulose, and silicon oil mounting (Faegri and Iversen, 1989). Pollen counts aimed 300 terrestrial pollen grains whenever that was possible. The abundance of terrestrial and aquatic pollen, as well as fern and fungal spores, was presented as a percentage of their respective total plus the sum of all terrestrial taxa. Pollen accumulation rates were also calculated using the SAR provided by the age-depth model and expressed as grains cm^{-2} yr^{-1}. Similarly, microscopic (<250 μm) charcoal particle were also counted and presented as charcoal accumulation rates (microscopic CHAR) using the aforementioned sedimentation rates. Main pollen trends were established by a stratigraphically constrained cluster analysis (CONISS) on all terrestrial taxa exceeding 4% using the software Tilia (Grimm, 1987). We further investigate trends in terrestrial vegetation by performing a Principal Component Analysis (PCA) on terrestrial pollen percentages, for which only taxa exceeding 4% of abundance were used. PCA analysis was performed with the aid of the R-studio platform (R Core Team, 2014).

The interpretation of the pollen record was based on the documented relationship between vegetation, elevation and summer precipitation in the western Andes slopes of northern Chile (Collao-Alvarado et al., 2015; de Porras et al., 2017; Jara et al., 2019; Latorre et al., 2002; Villagrán et al., 1981; see section 2.2). In mountainous regions, pollen is able to be transported both up and downslope over considerable distances, and therefore variations in pollen assemblages in high-elevation lakes can be interpreted as altitudinal shifts in vegetation (Markgraf, 1980). Consequently, a rise in pollen indicators of Prepuna and Puna taxa (e.g. Amaranthaceae, *Ephedra*, Brassicaceae or Ast. *Senecio* type) was interpreted as an upslope expansion in vegetation driven by drier conditions, whilst elevated percentages of high-Andean and Subnival pollen taxa (e.g. Poaceae, A. *Azorella* type or *Polylepis*) were interpreted as an expansion of highland vegetation in response to greater regional precipitation. Terrestrial pollen accumulation was associated to the degree of vegetation cover or plant productivity, which in the Andes of northern Chile is largely controlled by precipitation (Latorre et al., 2002). Yet, in continuous sedimentary sequences this variable can also be controlled by high-magnitude changes in the sediment accumulation rate. Temperature changes may favour the upward expansion of xerophytic species; however, an increment in precipitation is compulsory for the downward expansion of moist-sensitive Andean taxa to the Atacama Desert (Díaz et al., 2019). The interpretation of *Pediastrum* (Hydrodictyaceae), a genus of pelagic colonial green algae, is complex and regionally variable (Jankovská and Komárek, 2000). Hoverer, this genus can confidently be interpreted as a proxy for changing lake levels in tropical south America (Whitney and Mayle, 2012). In high-Andean lakes, *Pediastrum* grows preferably at low saline conditions in water depth between 4 and 10 m (Grosjean et al., 2001), and therefore at a shallow Andean lake such as LC high (low) *Pediastrum* abundances were more likely associated with relatively high (low) lake stands.

We further analysed past precipitation trends at LC by calculating a *Pollen Moisture Index* (PMI). The PMI is a numerical ratio of the relative abundance of high-Andean and Subnival versus Puna and Prepuna vegetation. Specifically, the index corresponded to the z-score of the ratio between the sum of Poaceae, A. *Azorella* type and *Polylepis* (high-Andean and Subnival) to the sum of Amaranthaceae, Ast. *Senecio* type, Ast. *Baccharis*, Ast. *Ambrosia* type, *Ephedra* and Brassicaceae (Puna and Prepuna). In other words, the PMI provided an indication of the relative dominance of high versus lowland vegetation, expressed as standard deviations from the record mean. Thus, positive PMI values indicated the dominance of high-Andean and Subnival (Puna and Prepuna) vegetation under relatively humid (dry) conditions.

4. Results

4.1. Stratigraphy and chronology

The sediment sequence from SHC-2 comprises 43.5 cm of homogeneous silts, grading from light-brown silts in the bottom 40 cm to dark-brown silt in the top three cm (Fig. 2). Organic density ranges from 0.06 to 0.08 g cm^{-3} throughout lower 40 cm, and then increases rapidly to values ranging from 0.12 to 0.18 g cm^{-3} over the top 4 cm. Carbonate content is constant through the core, ranging from 2 to 3%. The chronology of the sediment sequence is constrained by 6 AMS radiocarbon dates which show no reversal, suggesting continuous deposition over the last 4070 years (2 σ modelled range = 3820–4582 cal yr BP) (Fig. 3; Table 1). The top-most cm provides a modern radiocarbon age, thereby modern reservoir effect is negligible. Low and constant carbonate content summed to the absence of stratigraphic and geomorphological evidence for a significant reduction in the modern volume of the lake, suggests that the reservoir effect remained negligible over the past (Giralt et al., 2008). Sediment Accumulation Rate (SAR) ranges from 0.004 to 0.036 cm year $^{-1}$ (record mean = 0.017 cm year $^{-1}$), with two period of increased accumulation between 44.5 and 30 cm (4000-3600 cal yr BP) and between 20.5 and 12 cm (2400-1600 cal yr BP) (Fig. 3; Table 2). There is not significant correlation between organic density and SAR changes (Pearson correlation coefficient r = −0.19; p-value = 0.06), indicating that intervals of increased sedimentation did not result from higher organic productivity but from the precipitation-driven slope outwash around the lake.

4.2. Pollen record

The pollen sequence of Laguna Ceusis comprises 86 samples with a mean sample resolution of 48 years (Fig. 4). The sequence presents very low pollen concentration (mean total terrestrial

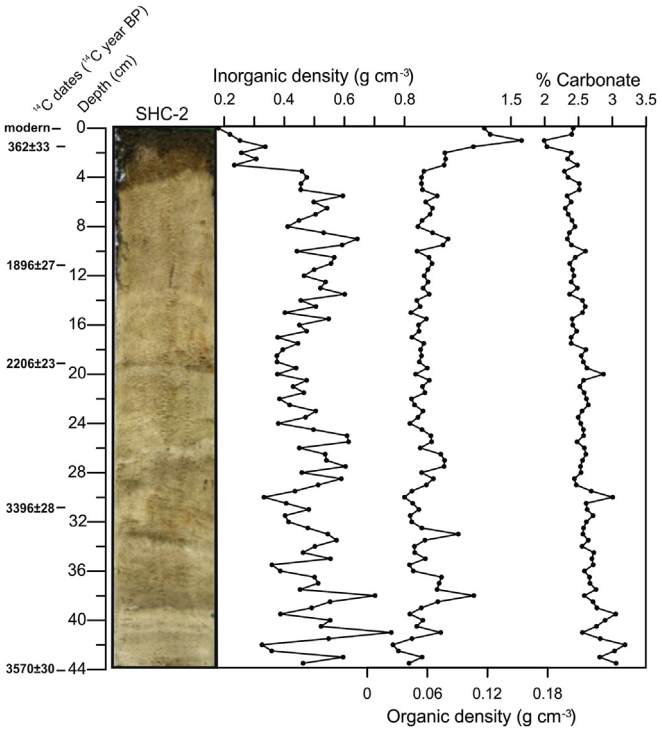

Fig. 2. Profile of Short Core 2 (SHC2) from Laguna Ceusis, including the position of all radiocarbon dated levels on the right. Organic and inorganic density obtained from the Loss on Ignition analysis are plotted on the left along with the percentage of carbonates.

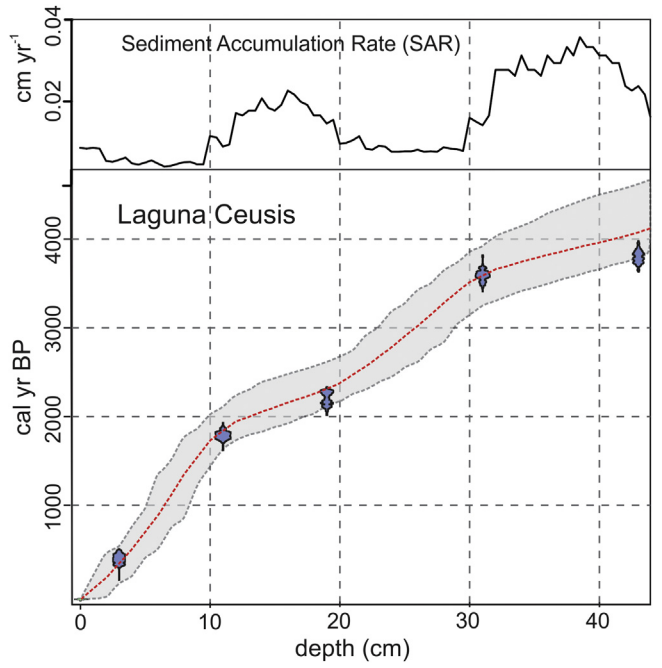

Fig. 3. Laguna Ceusis Bayesian age-depth model. Calendar age distributions for each date are shown in blue. 95% confidence limits for the entire section are enclosed in light grey. The red line corresponds to the weighted mean calendar age for the entire section. Sediment Accumulation Rate (SAR) values are depicted in the upper panel.

concentration = 5303 grain cm^{-3}), which is expected considering the sparse vegetation around the lake as a result of the arid and cold Andean environment. At least 300 pollen grains were identified in 73 of the 86 samples (85%). Samples that did not reach that pollen count averaged 268 grains. The pollen record is largely dominated by Amaranthaceae (mean abundance = 35%), Poaceae (29%) and Ast. *Senecio* type (10%), with abundant *Pediastrum* (60%) and *Sporormiella* fungal spores (3%) (Fig. 4). We distinguish 6 main zones based on the CONISS ordination (zones LC-1 to LC-6), which are shown in Fig. 4 and described in detail in Table 2. Principal Component axis 1 (PC1) explains 27% of the total variance of dominant terrestrial pollen types, and exhibits strong positive loadings for Poaceae, Amaranthaceae and A. *Azorella* type, and negative loadings for Ast. *Senecio* type, Ast *Baccharis* type and Ast. *Ambrosia* type (Fig. 5, right panel). Principal Component axis 2 (PC2), on the other hand, explains 17% of the variance and contrasts strong positive loadings for Brassicaceae, Amaranthaceae and *Ephedra* with negative loadings for *Polylepis* and Poaceae. Samples from all zones exhibit near-zero or positive values of PC1, with the exception of zone LC-6 which shows strong negative PC1 scores. Zone LC-2 and LC-3 show slighter higher PC2 scores; while zone LC-4 shows slightly lower values (Fig. 5; left panel).Total terrestrial pollen accumulation averages 87 grain cm^{-2} yr^{-1}, with two periods of enhanced accumulation between 4000–3600 and 2200-1600 cal yr BP (Fig. S1). Strong positive correlation between terrestrial pollen accumulation and SAR ($r = 0.92$; p-value < 0.01) indicates, however, that pollen accumulation rates are subject to the high-magnitude changes in the SAR. Microscopic CHAR variations shows very similar trends to the terrestrial pollen accumulation and, expectedly, CHAR values are also highly correlated with the SAR ($r = 0.72$; p-value <0.01), indicating that charcoal accumulation is controlled by the sedimentological variations in the lake. Hence, the ecological and climatic interpretations based on pollen and charcoal accumulation trends should be viewed with caution and evaluated in the light of other ecological and/or sedimentological variables not affected by the SAR (i.e., percentage or concentration data). Despite these covariations at the accumulation level, no statistical correlation between charcoal and pollen concentrations is found, suggesting the absence of an underlying, long-term fire-vegetation relationship. Percentages of *Pediastrum* are also significantly correlated with the SAR ($r = 0.45$; p-value <0.01). However, these two are independent variables, and therefore their correlation implies that precipitation-driven SAR and *Pediastrum* abundances covaried throughout the record, supporting the published evidence indicating that *Pediastrum* can be used as a reliable lake level indicator (Whitney and Mayle, 2012).

4.3. Pollen Moisture Index

The PMI reveals six intervals in which five or more adjacent samples exhibit positive or negative scores. Consecutive positive values are observed between 3800–3700, 3600–3400 and 2300-1900 cal yr BP and are associated with the preeminence of high Andean and Subnival vegetation; whereas negative scores are recorded between 2500–2300, 1400-1000 cal yr BP and over the last 400 years, reflecting the preeminence of Puna and Prepuna vegetation (Fig. 4). Four PMI samples show scores that are two standard deviations above the record mean at ~4000, 3800, 3400 and 2200 cal yr BP, located in the context of positive centennial-scale anomalies; whereas one sample falls below two standard deviations at 130 cal yr BP, within the most recent negative centennial-scale anomaly (Fig. 6a, red dots).

Despite of being independent variables, positive correlation between the SAR and the PMI ($r = 0.34$; p-value <0.01) indicates that periods of increased (decreased) sedimentation tend to be associated with overall dominance of high-Andean (Puna and Prepuna) vegetation, thereby both the SAR and PMI represent two independent regional precipitation proxies.

Table 1
Radiocarbon-dated levels from core SHC-2 of Laguna Ceusis. All dates were obtained from bulk sediments.

Laboratory Code	core length (cm)	^{14}C yr BP	1 σ error	median probability (cal yr BP)	youngest 2 σ intercept (cal yr BP)	oldest 2 σ intercept (cal yr BP)
D-AMS 018464	1–2	modern				
D-AMS 032835	3–3.5	362	33	392	308	485
D-AMS 028563	11–12	1896	27	1787	1719	1870
D-AMS 028564	19–20	2206	23	2179	2090	2306
D-AMS 028565	31–32	3396	28	3594	3481	3689
D-AMS 018465	43–43.5	3570	30	3900	3696	4152

Table 2
Zones of Laguna Ceusis pollen record. Zonation was based on the CONISS analysis.

Zone	N° of Samples	Stratigraphic position (cm)	Age range (cal yr BP)	Mean sediment accumulation rate (cm yr-1)	Dominant taxa and PMI (zone mean)	Description
LC-1	**28**	**44-29**	**4100-3400**	**0.025**	Amaranthaceae (35%), Poaceae (30%), Ast. *Senecio* type (9%). PMI = 0.44	Highly variable abundances of all taxa. Relative high percentages of Poaceae, A. *Azorella* type and *Polylepis* and peak values of *Pediastrum*. Marked peaks in terrestrial pollen accumulation and microscopic CHAR
LC-2	**9**	**29-24.5**	**3400-2800**	**0.008**	Amaranthaceae (38%), Poaceae (28%), Ast. *Senecio* type (9%). PMI = -0.26	No significant variations in any major taxa, apart from a sustained decline of *Pediastrum* and successive peaks in Ast. *Baccharis* type, Ast. *Ambrosia* type and Brassicaceae between 3400 and 3100 cal yr BP. Minimum values of terrestrial pollen accumulation and microscopic CHAR
LC-3	**11**	**24.5-19**	**2800-2300**	**0.011**	Amaranthaceae (39%), Poaceae (25%), Ast. *Senecio* type (10%). PMI = -0.81	Sustained rises in Amaranthaceae and Brassicaceae and drop in A. *Azorella* type. Peaks in Ast. *Senecio* type, *Ephedra*, Ast. Mutisieae. Minimum values in *Pediastrum*. Terrestrial pollen accumulation and microscopic CHAR exhibit minimum values
LC-4	**14**	**19-12**	**2300-1900**	**0.019**	Amaranthaceae (34%), Poaceae (34%), Ast. *Senecio* type (8%). PMI = 0.82	Rapid drops of Amaranthaceae and *Ephedra*. Increases in Poaceae, A. *Azorella* type and *Polylepis*. Peak abundances of terrestrial pollen accumulation and microscopic CHAR and *Pediastrum*
LC-5	**16**	**12-4**	**1900-500**	**0.006**	Amaranthaceae (35%), Poaceae (29%), Ast. *Senecio* type (10%). PMI = -0.17	Long-term increases in Ast. *Senecio* type and Brassicaceae and sustained drop in Poaceae. Single peaks in Ast. Mutisieae and Ast. *Ambrosia* type. Long-term drop in terrestrial pollen accumulation and near-zero microscopic CHAR values. Increase in *Pediastrum*
LC-6	**8**	**4-0**	**500- -65**	**0.007**	Amaranthaceae (25%) Ast. *Senecio* type (23), Poaceae (21%). PMI = -1.43	Rapid rises in Ast. *Senecio* type, Ast. *Ambrosia* type, Ast. *Baccharis* type and A. *Schinus* type. Sustained drops in Amaranthaceae, Poaceae and A. *Azorella* type. Minimum values of terrestrial pollen accumulation and microscopic CHAR. Peaks in *Pediastrum* and *Sporormiella* fungal spores

5. Discussion

5.1. Vegetation and climate reconstruction

The pollen sequence of LC allows a detailed assessment of the late Holocene vegetation and climate history in the Andes of northern Chile. The great majority of pollen taxa show highly variable percentages between 4000 and 3400 cal yr BP, which is likely due to the higher sample resolution of this interval (Fig. 4; zone LC-1). Superimposed to this variability, we distinguish overall high percentages of the cushion plant A. *Azorella* type and the high-Andean tree *Polylepis*, followed by an expansion of Poaceae between 3600 and 3400 cal yr BP. These palynological trends suggest a long-term expansion of high-altitude vegetation in response to increasing regional humidity. Tree ring chronologies from the Altiplano are consistent with this interpretation, showing that *Polylepis* is favoured by persistent wet conditions (Morales et al., 2012). High SAR values during this interval are also consistent with our climate inference, indicating a period of heightened slope wash around the lake (Fig. 3). Sediment accumulation at LC could have been further enhanced by the long-term accumulation of terrigenous material after an extended interval of reduced regional precipitation in the Andes of northern Chile between ~8000 and 4000 cal yr BP (de Porras et al., 2017; Pueyo et al., 2011). High peaks in pollen and microscopic charcoal accumulation during this interval are not accompanied by corresponding increments in pollen and charcoal concentrations (Fig. S1), and therefore accumulation values reflect the dominant influence of the SAR. Increasing rainfall and slope runoff could have contributed to the relatively elevated lake levels indicated by high *Pediastrum* abundances (Fig. 4). These changes are clearly visible in the PCA plots in which LC-1 samples are grouped in the proximities of A. *Azorella* type (Fig. 5) and around SAR and *Pediastrum* (Fig. S2). In sum, increases in high-Andean vegetation, raised rates of sediment accumulation and high lake levels suggest enhanced precipitation between 4000 and 3400 cal yr BP.

A series of minor expansions of Ast. *Baccharis* type, Ast. *Ambrosia* type and Brassicaceae are observed between 3400 and 3000 cal yr BP. This succession is followed by two prominent albeit short-lived peaks of Ast. *Senecio* type and Ast. *Baccharis* type at ~2800 cal yr BP, and by expansions of Amaranthaceae and *Ephedra* between 2700 and 2400 cal yr BP (Fig. 4; zones LC-2 and LC-3). These changes are visible as increments of Prepuna and Puna pollen in Fig. 4, pointing to an upward expansion of xerophytic vegetation. Recent investigations on the climate controls of the regional flora shows that changes in the elevation of perennial shrubs can only result from long-term climate alterations (Díaz et al., 2019). We interpret the expansion of Puna and Prepuna shrubs as resulting from a long-term drying trend. Consistent with this interpretation, a rapid drop in the SAR at 3600 cal yr BP indicates decreasing surface runoff (Fig. 3), while sustained reductions in *Pediastrum* abundances and the presence of traces of the littoral taxa Cyperaceae indicate a drop in lake levels and the expansion of shallow-water vegetation respectively (Fig. 4). These series of changes are summarized in the PCA plot with a significant displacement of LC-2 and LC-3 samples toward higher PC2 values, which are now located closer to the

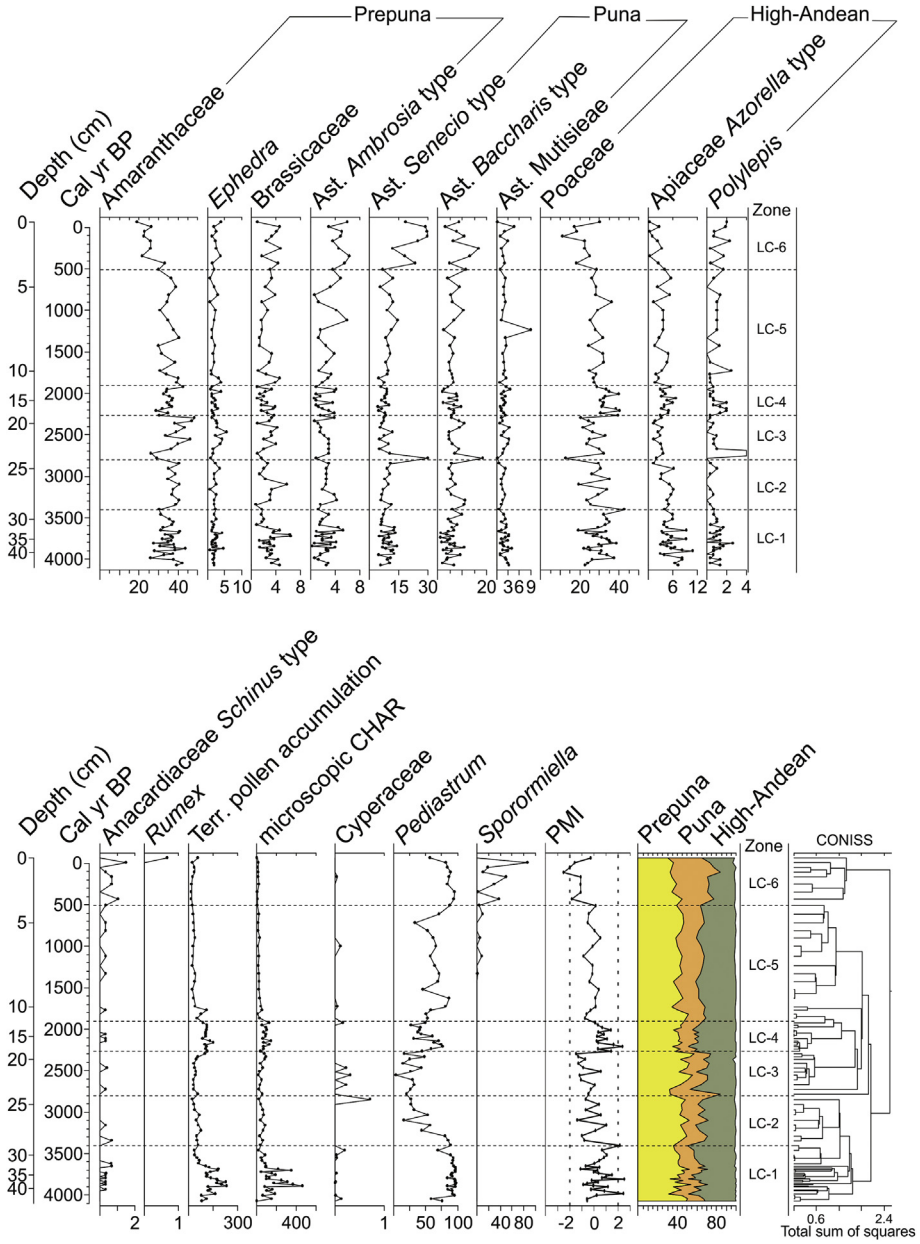

Fig. 4. Pollen record from Laguna Ceusis. Temporal and stratigraphic changes in the percentage of main terrestrial and aquatic taxa. Terrestrial pollen and microscopic charcoal accumulation rates are also included (lower panel). Pollen zones are shown on the right area on both panels, whilst CONISS analysis is plotted on the lower panel.

Prepuna shrubs (Fig. 5). In short, we interpret this evidence as a progressive upslope displacement of lower vegetation belts, reduced surface runoff and lower lake levels in response to declining precipitation between 3400 and 2300 cal yr BP.

The high-Andean taxa Poaceae and A. *Azorella* type show elevated abundances between 2300 and 1900 cal yr BP. These increments occur at expenses of Prepuna and Puna indicators, chiefly Amaranthaceae and *Ephedra*, indicating a relative expansion of high-Andean vegetation under higher regional precipitation (Fig. 4; zone LC-4). Supporting such interpretation, a new increase of the SAR indicates a reinvigoration of slope runoff around the lake, while raising lake levels are inferred from a rapid recovery of *Pediastrum* percentages. In the PCA plot these changes are depicted as a displacement of LC-4 samples toward lower values in PC2, closer to the high-Andean taxa (Fig. 5). In response to increased SAR, terrestrial pollen accumulation experiences a significant increment between 2300 and 1800 cal yr BP. Yet, the concentration of high-Andean pollen taxa also increases rapidly during this interval (Fig. S1, zone LC-4), indicating that the heightened accumulation rates of such taxa are not only driven by the SAR but also reflecting a genuine pulse of increasing vegetation cover and terrestrial productivity. Taken together, expanded high-Andean vegetation, increased sedimentation rates, and heightened lake levels indicate a period of high precipitation between 2300 and 1900 cal yr BP.

Most pollen indicators are unchanged between 2000 and 700 cal yr BP, which suggests a period of relative climate stability without any clear centennial-scale excursion. This constancy is only interrupted by a long-term increasing trend of Brassicaceae starting at 1600 cal yr BP and by successive expansions of Ast. *Baccharis* type and Ast. *Ambrosia* type at 1400 and 900 cal yr BP respectively (Fig. 4; zone LC-5). These trends are seen in the PCA plot as an

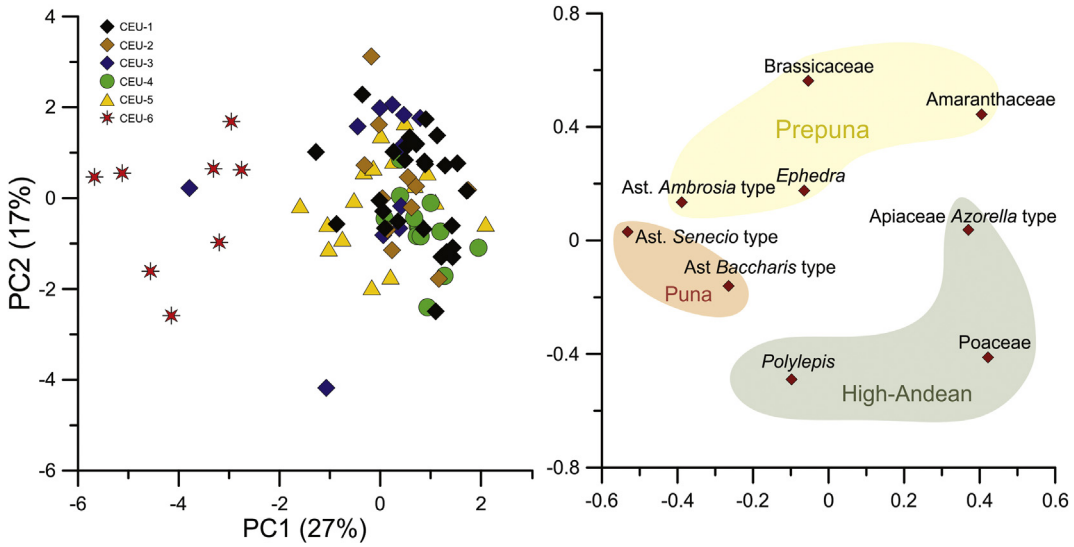

Fig. 5. Summary plot of the Principal Component Analysis (PCA) performed on the terrestrial pollen dataset of Laguna Ceusis. Sample scores are presented in the left panel while Taxa loadings are shown on the right.

overall shift towards higher PC2 values in the LC-5 sample scores, which are now positioned closer to the aforementioned Prepuna and Puna taxa (Fig. 5). The position of the LC-5 samples in the PCA plot is, nonetheless, intermediate between the dry assemblages of LC-2 and LC-3 and the humid assemblages of LC-4 samples. Low SAR values after 1600 cal yr BP are indicative of diminished surface runoff. Interestingly, the low pollen accumulation rates observed in Fig. 4 are largely driven by the diminished SAR and contrast with relatively high pollen concentration values (Fig. S1), suggesting an interval of increased vegetation cover. This later interpretation is consistent with the elevated percentages of high-Andean taxa and *Pediastrum* observed between 2000 and 700 cal yr BP, indicative of relatively humid conditions and high lake levels (Fig. 4). In sum, the LC precipitation proxies do not show an unequivocal trend, which likely resulted from a period of intermediate rainfall regimes. Interestingly, the LC record does not show any significant vegetation or sediment accumulation anomalies during the MCA chronozone (Fig. 6).

The last 500 years of the record are marked by a rapid increment of the perennial shrubs *Ephedra,* Ast. *Baccharis* type, Ast. *Ambrosia* type, followed by a prominent expansion of Ast. *Senecio* type in the last 200 years (Fig. 4; zone LC-6). Minor expansions of the arboreal taxa *Polylepis* and Anacardiaceae *Schinus* type are also observed during this interval, along with a rise in Poaceae in the last 130 years. Amaranthaceae and A. *Azorella* type, on the other hand, experienced sustained drops. This interval also features a rapid increase in the coprophilous fungus *Sporormiella*, which more likely reflects the presence of browsing herbivores, camelids and/or non-native species, around the lake. These changes are clearly summarized in the PCA plots by a marked shift towards lower PC1 scores in all LC-6 samples, which are now closer to Ast. *Senecio* and Ast. *Baccharis* type (Fig. 5); and by a closer affinity of LC-6 samples with *Sporormiella* (Fig. S2). While Prepuna shrubs such as Ast. *Baccharis* and Ast. *Ambrosia* types could certainly be interpreted as dry indicators, the latter expansion of Ast. *Senecio* type should be taken cautiously because this pollen type includes the high elevation taxon *Parastrephia* spp., which occurs in the LC catchment today. In fact, the Ast. *Senecio* type expansion at LC corresponds well with a period of increased Ast. *Parastrephia* pollen in fossil rodent middens in the Andes of northern Chile, interpreted as reflecting enhanced rainfall (Mujica et al., 2015; 18°S; 3000–3500 masl). Yet, we note that this pollen trend is documented several hundred meter below our study site. At LC, other humid indicators include raised arboreal taxa, relative high lake levels indicated by abundant *Pediastrum* (Fig. 4), and a minor rise in the SAR (Fig. 2). Although these changes could reflect the onset of more humid conditions -which in this case could be correlated to increased precipitation documented in the western flanks of the central Andes during the LIA (Morales et al., 2012), and more generally in the entire domain of the SASM influence (Campos et al., 2019)- we caution about this interpretation because the anthropogenic signature in the LC record did more likely override any regional climate signal. A recent integration of archaeological and paleoenvironmental records shows that the Andes of northern Chile experienced a dramatic population growth over the last 600 years (Gayo et al., 2019). In this scenario, the marked increments in Asteraceae perennial shrubs at LC could be explained by more intense and/or frequent anthropogenic activities in the high Andes during the most recent centuries. The introduction of hard-hoover cattle to the catchment could have favoured the expansion of perennial shrubs by promoting vegetation removal and catchment erosion, and by removing grasses due to browsing dietary preferences (Hooper et al., 2020). Furthermore, anthropogenic erosion including herbivorous herding could have explained part of the rise in the SAR, while heightened *Pediastrum* abundances could have been driven by the rapid pulse of lake eutrophication inferred by the increase in organic sedimentation (Fig. 2). Mining activities could also have contributed to the rise in organic sedimentation observed over the most recent centuries, as LC is located less than 10 km from a large mining complex.

5.2. Temporal and spatial patterns of past SASM precipitation

The overwhelming contribution of SASM precipitation in the study area assures that the reconstructed pollen-precipitation trends from LC reflect past changes in monsoonal activity. Fig. 6a and b presents the PMI and the SAR curves, two independent precipitation proxies from LC. A former interval of largely positive PMI values coincides with a prominent peak in the SAR between 4000 and 3400 cal yr BP, suggesting a well-defined period of enhanced SASM precipitation. In fact, two independent short-term humid pulses are identified in the PMI at 3800 and 3600 cal yr BP,

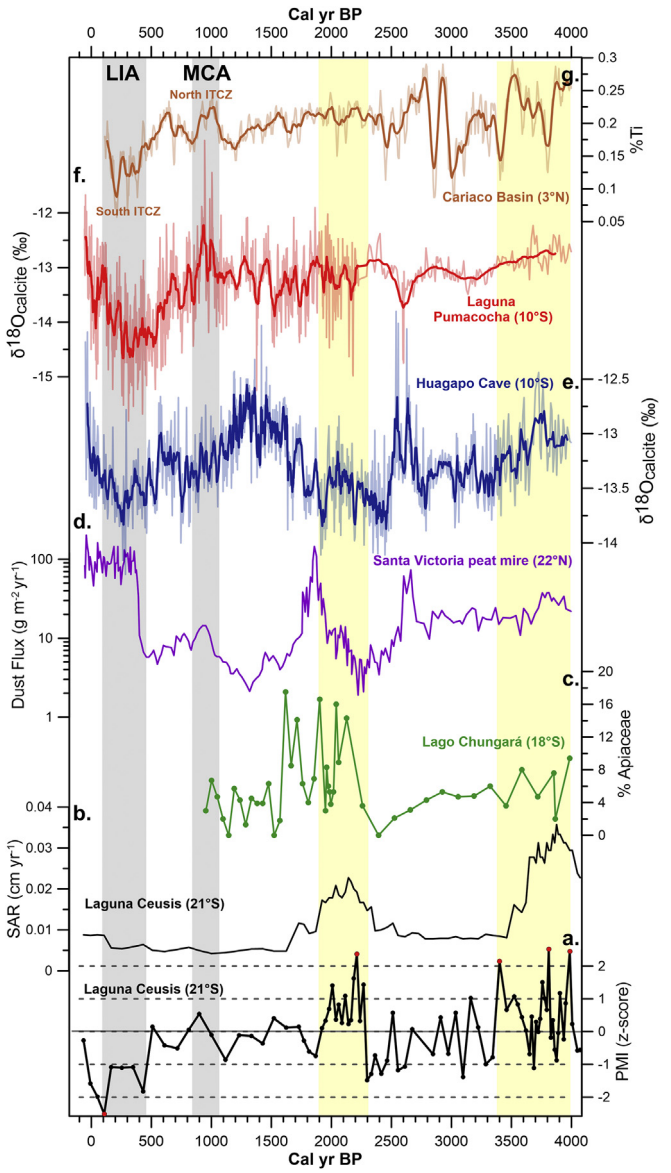

Fig. 6. Summary of Laguna Ceusis precipitation proxies along with other SASM reconstructions discussed in the main text. (a) Z-scores of Laguna Ceusis Pollen Moisture Index (PMI), $+2\sigma/-2\sigma$ scores highlighted in red, (b) Laguna Ceusis Sediment Accumulation Rate (cm yr^{-1}). (c) Lago Chungará Apiaceae percentages (Jara et al., 2019), (d) Dust flux record from Santa Victoria peat mire (Hooper et al., 2020), (e) Huagapo Cave isotopic record with 5-point weighted averages (Kanner et al., 2013), (f) Laguna Pumacocha isotopic record with 17-point weighted averages (Bird et al., 2011 holocene), (g) Cariaco Basin Titanium record with 11-point weighted averages (Haug et al., 2001). Vertical yellow bars correspond to the two humid intervals detected at Laguna Ceusis (LC). Medieval Climate Anomaly (MCA) and the Little Ice Age (LIA) shown in light grey vertical bars.

although those pulses are not distinguished in the SAR curve. This multi-centennial humid anomaly might correspond with the onset of a period of increased rainfall recorded after 4000 cal yr BP in Laguna Miscanti, on the high Andes 330 km south from LC (Grosjean et al., 2001), and also with overall high lake levels recorded over the last 5000 years at Lago Chungará, 310 km north from LC (Sáez et al., 2007, Fig. 1a). However, pollen, ostracod valves, diatoms and endogenic carbonates from this latter Andean lake suggest that arid conditions may have persisted until 3300 cal yr BP (Jara et al., 2019; Pueyo et al., 2011, Fig. 6c). The early humid anomaly at LC is also correlated with an increase in grass remains observed between 4300 and 3200 cal yr BP in fossil rodent middens from the Atacama Desert (22°S; Latorre et al., 2003), as well as the onset of dry conditions by 3500 cal yr BP inferred from the incision of wetland deposits, 160 km south from LC (Tully et al., 2019). By contrast, enriched isotopic values are observed between 4000 and 3600 cal yr BP in the Huagapo Cave and Laguna Pumacocha records (10°S; Fig. 1a; approximately 1300 km to the northwest of LC.), indicating that overall weakened monsoon and dry conditions prevailed in the Tropical Andes (Bird et al., 2011a; Kanner et al., 2013, Fig. 6e and f). A northerly position of the ITCZ is suggested by high Ti percentages in the Cariaco Basin (Haug et al., 2001, Fig. 6g), consistent with the tropical Andes reconstructions mentioned above; even though a short-lived southward shift can be inferred from a brief drop in Ti between 3850 and 3700 cal yr BP. Nonetheless, these differences suggest that the multi-centennial interval of enhanced SASM precipitation observed at LC and records from the Andes of northern Chile and the Atacama Desert roughly between 4000 and 3500 cal yr BP did not extend into the tropical Andes, and that it was largely decoupled from latitudinal ITCZ variations.

A latter humid anomaly at LC is indicated by the PMI and the SAR curves between 2300 and 1900 cal yr BP, and appears to be recognized in several records from the Andes of northern Chile and the Atacama Desert. For instance, it is clearly observed at Lago Chungará in the form of prominent increments in the high-Andean taxon Apiaceae between 2400 and 1600 cal yr BP (Fig. 6c). Although the high Andean pollen expansion at Lago Chungará postdates in a few centuries the above-mean PMI values recorded at LC (Fig. 6a), such a difference may be explained by the uncertainties derived from the Lago Chungará chronology (Giralt et al., 2008). Nonetheless, the Chungará Apiaceae increment matches the peak in SAR values (Fig. 6b), indicating a synchronic SASM precipitation signal. In addition, increments in grass remains in fossil rodent middens in the upper margins of the Atacama Desert (23°S; 2600–2800 masl) indicate a surge in summer rainfall by 2000 cal yr BP (Latorre et al., 2002); while a major increment of Poaceae pollen in middens from the western Andes flanks, 100 km north from LC (20°S; 3750 masl), reveals increased precipitation between 2200 and 1100 cal yr BP (Maldonado and Uribe, 2012). The presence of abundant plant remains and extensive wetland deposits in the hyperarid core of the Atacama Desert (21–22°S; 1000–2700 masl) suggest heightened regional moisture between 2500 and 2000 cal yr BP (Gayo et al., 2012) and between 2700 and 1300 cal yr BP (Rech et al., 2003; Tully et al., 2019).

The most recent LC humid anomaly is also matched by records from the eastern flanks of the central Andes. For instance, a reinvigoration of SASM precipitation between 2600 and 1700 cal yr BP is inferred from an increment in peat accumulation, a rise in Poaceae pollen, and a significant drop in westerly dust fluxes in the Santa Victoria peat mire (Hooper et al., 2020; 22°S; Fig. 6d); whilst enhanced regional moisture is inferred from a depletion of $\delta^{18}O$ values between 2100 and 1750 cal yr BP in the Cerro Tuzgle cushion peatland (Kock et al., 2019; 24°S; Fig. 1a). Furthermore, this widely recorded centennial-scale event may be related to a shift towards higher SASM precipitation at 2400 cal yr BP in the core of the central Andes, as revealed by a depletion in Deuterium values in sediments from Lake Titicaca (15°S; Fornace et al., 2014). Further north, the LC humid anomaly agrees with overall greater monsoon precipitation inferred by depleted $\delta^{18}O$ values at Huagapo Cave between 2400 and 1600 cal yr BP (Fig. 6e). However, no isotopic depletion is seen at Laguna Pumacocha during this time (Fig. 6f), and relatively high Ti percentages in the Cariaco Basin indicate an overall northerly position of the thermal equator (Fig. 6g). Interestingly, a recently published isotopic record from plant waxes shows humid conditions between 2450 and 1550 cal yr BP at

Boqueirão Lake in northeastern Brasil (Utida et al., 2019; 5°S; Fig. 1a). Despite potential dating uncertainties, coherence between proxy records from the western and eastern central Andes suggests a widespread humid event roughly between 2500 and 1700 cal yr BP. Comparisons with the Cariaco record indicate that this humid event was not associated to a southward shift of the ITCZ; and thereby related to a different moisture source. With the exception of the Huagapo Cave record, we note that humid conditions started early and/or were more conspicuous in the western and eastern flanks of the southern central Andes (>18°S), suggesting an intensification of SASM precipitation from south to north, more likely derived from a southerly moisture source.

5.3. Sources and mechanisms of past SASM precipitation

Temperature variations in the tropical Pacific Ocean are one of the most important drivers of modern SASM variability in the central Andes from interannual to multi-decadal timescales (Garreaud et al., 2009; Segura et al., 2016). Hence, it might be expected that the multi-centennial pluvial events recorded at LC as well as the temporal and spatial trends identified in reconstructions from the tropical, centra Andes and the Atacama Desert resulted from past ENSO-like variability. However, we note that modern ENSO variability causes distinctive precipitation anomalies between the eastern and western sides of the Andes cordillera, that is, humid (dry) conditions prevail in the Pacific coast in opposition to dry (humid) conditions eastward from the Andes divide during canonical eastern Pacific El Niño (La Niña) years (Sulca et al., 2016). If past ENSO-like variability was the driving force of late Holocene SASM precipitation in the central Andes, the spatial variability seen in proxy records should exhibit a west-east instead of the north-south gradient described above. Furthermore, it has been shown that the modern ENSO-SASM precipitation relationship cannot explain the late Holocene SASM anomalies observed in proxy records (Jara et al., 2019; Vuille et al., 2012), and therefore changes in the tropical Pacific are unlikely to be the dominant force behind the past centennial-scale trends discussed in the previous section.

Differences in paleoclimatic trends between records from the central and tropical Andes have already been highlighted in a recent reconstruction from the Umajalanta–Chiflonkhakha cave system in the eastern flanks of the central Andes (Apaéstegui et al., 2018; 18°S; Fig. 1a). Apaéstegui et al. (2018) show that a centennial-scale event of enhanced precipitation in this region can be explained by the transport of moisture from the southern tropical Atlantic through the southern Amazon basin and southeastern South America, meanwhile the ITCZ remained in a northerly position. This mechanism is not only consistent with the LC pluvial events and the spatial patterns revealed in our proxy comparisons, but also with modern climatological studies showing that different modes of SASM precipitation can produce significant spatial variability between the northern and southern SASM domains at interannual timescales (Vuille and Keimig, 2004). In particular, a "southeasterly mode" can be generated by a southward displacement of the Bolivian high, leading to enhanced precipitation in the southern central Andes. A similar mechanism was identified earlier by Lenters and Cook (1999) using global atmospheric datasets. These authors showed that Rossby wave dispersion from the Southern Hemisphere extra-tropics may lead to a southward position of the Bolivian high and a strengthening of the SACZ during summer months, thereby promoting the advection of moist air masses towards the southern portion of the central Andes. In addition, positive hydrological anomalies in the southern central Andes can result from an increase in sea surface temperatures over the southern Atlantic Ocean, which will weaken the SACZ but promote the intrusion of extra-tropical cold fronts through La Plata Basin further south (Campos et al., 2019, Fig. 1a). This latter mechanism has been observed in satellite rainfall observations, fostering the propagation of rainfall through the Argentinian planes and becoming an important component of present-day precipitation in the southern central Andes (Boers et al., 2016). Interestingly, this mechanism would also result in humid conditions in northeastern Brazil, consistent with the late Holocene anomaly documented by Ultida et al. (2019). In summary, at least two different -although not mutually exclusive- mechanisms could explain the multi-centennial humid events detected at LC as well as the spatial configuration of SASM precipitation anomalies revealed by the paleoclimate records discussed here. New late Holocene reconstructions from the central Andes and southeastern South America are undoubtedly needed to better constrain the amplitude, spatiotemporal evolution, and mechanisms of late Holocene SASM precipitation.

6. Conclusions

The pollen and sediment accumulation records from LC show that important changes in vegetation and climate occurred in the dry Andes of northern Chile over the last 4000 years, and demonstrate that the central Andes region experienced well-defined centennial-scale anomalies in SASM precipitation prior to the LIA and MCA. In particular, we distinguished two episodes of significantly enhanced SASM precipitation between 4000–3400 and 2300-1900 cal yr BP. A comparison of these precipitation episodes with reconstructions from the entire domain of the monsoon provides new evidence for the temporal and spatial variability of the SASM. Correspondence between LC and several records from the central Andes suggests the occurrence of two widespread pluvial events between ~4000–3500 and ~2500-1700 cal yr BP, largely decoupled from latitudinal shifts of the ITCZ and therefore not directly related to the tropical drivers that controlled SASM variations during the LIA and MCA. Based on the modern drivers and spatial variability of the SASM, the most plausible explanation for these past precipitation episodes is an intensification of the SACZ and/or the intrusion of convective activity from southeastern South America. Further climate reconstructions and modelling experiments are needed to refine the chronologies and mechanisms of paleoclimate change proposed in this study. Nonetheless, the LC record shows that the drivers, temporal evolution, and spatial variations of late Holocene monsoonal precipitation in the central Andes were considerably more diverse than previously thought. Hence, caution should be taken in assuming that the range of hydrological variability documented in the instrumental record so far will persist in the future.

Declaration of competing interest

The authors declare that they have no known competing financial interests or personal relationships that could have appeared to influence the work reported in this paper.

Acknowledgements

We thank Claudia Alcaíno for her support during the Loss on Ignition data acquisition at CEAZA, Jeremy Acevedo Cortés for field assistance and two anonymous reviewers whose comments helped to improve this manuscript. This investigation was funded by FONDECYT postdoctoral grant # 3190181 and FONDECYT # 1181829.

Appendix A. Supplementary data

Supplementary data to this article can be found online at https://doi.org/10.1016/j.quascirev.2020.106533.

Data availability

All published information included in the text is given with their respective references. The pollen data presented in this article will be freely available in the Neotoma paleoecological database (https://www.neotomadb.org/) once it is accepted for publication.

Author contribution

Ignacio A. Jara: Funding acquisition, Conceptualization, Methodology, Formal analysis, Investigation, Writing - original draft and Visualization, Writing - review & editing. Antonio Maldonado: Fieldwork, Funding acquisition, Conceptualization, Writing - review & editing, Supervision. María Eugenia de Porras: Fieldwork, Funding acquisition, Conceptualization, Writing - review & editing.

References

Aceituno, P., Montecinos, A., 1993. Circulation Anomalies Associated with Dry and Wet Periods in the South American Altiplano, Proc. Fourth Int. Conf. On Southern Hemisphere Meteorology. Amer. Meteor. Soc), pp. 330–331.

Apaéstegui, J., Cruz, F.W., Vuille, M., Fohlmeister, J., Espinoza, J.C., Sifeddine, A., Strikis, N., Guyot, J.L., Ventura, R., Cheng, H., 2018. Precipitation changes over the eastern Bolivian Andes inferred from speleothem (δ 18 O) records for the last 1400 years. Earth Planet Sci. Lett. 494, 124–134.

Baker, P.A., Fritz, S.C., 2015. Nature and causes of Quaternary climate variation of tropical South America. Quat. Sci. Rev. 124, 31–47.

Bird, B.W., Abbott, M.B., Rodbell, D.T., Vuille, M., 2011a. Holocene tropical South American hydroclimate revealed from a decadally resolved lake sediment δ18O record. Earth Planet Sci. Lett. 310, 192–202.

Bird, B.W., Abbott, M.B., Vuille, M., Rodbell, D.T., Stansell, N.D., Rosenmeier, M.F., 2011b. A 2,300-year-long annually resolved record of the South American summer monsoon from the Peruvian Andes. Proc. Natl. Acad. Sci. Unit. States Am. 108, 8583–8588.

Blaauw, M., Christen, J.A., 2011. Flexible paleoclimate age-depth models using an autoregressive gamma process. Bayesian analysis 457–474.

Boers, N., Bookhagen, B., Marwan, N., Kurths, J., 2016. Spatiotemporal characteristics and synchronization of extreme rainfall in South America with focus on the Andes Mountain range. Clim. Dynam. 46, 601–617.

Brush, S.B., 1982. The Natural and Human Environment of the Central Andes. Mountain Research and Development, pp. 19–38.

Bustamante, M., Cruz, F., Vuille, M., Apaéstegui, J., Strikis, N., Panizo, G., Novello, F., Deininger, M., Sifeddine, A., Cheng, H., 2016. Holocene changes in monsoon precipitation in the Andes of NE Peru based on δ18O speleothem records. Quat. Sci. Rev. 146, 274–287.

Campos, J., Cruz, F., Ambrizzi, T., Deininger, M., Vuille, M., Novello, V.F., Strikis, N., 2019. Coherent South American Monsoon variability during the last millennium revealed through high-resolution proxy records. Geophys. Res. Lett. 46, 8261–8270.

Canedo-Rosso, C., Uvo, C.B., Berndtsson, R., 2019. Precipitation variability and its relation to climate anomalies in the Bolivian Altiplano. Int. J. Climatol. 39, 2096–2107.

Cheng, H., Fleitmann, D., Edwards, R.L., Wang, X., Cruz, F.W., Auler, A.S., Mangini, A., Wang, Y., Kong, X., Burns, S.J., 2009. Timing and structure of the 8.2 kyr BP event inferred from δ18O records of stalagmites from China, Oman, and Brazil. Geology 37, 1007–1010.

Collao-Alvarado, K., Maldonado, A., González, L., Sandoval, A., De Porras, M.E., Zamora, A., Arancio, G., 2015. Estudio de la relación polen-vegetación actual en el Norte de Chile, en el transecto Pozo Almonte-Salar de Huasco (20°15'S/69°06'O). Gayana. Botánica 72, 125–136.

De Carvalho, L.M.V., Jones, C., 2015. The Monsoons and Climate Change: Observations and Modeling. Springer.

de Porras, M.E., Maldonado, A., De Pol-Holz, R., Latorre, C., Betancourt, J.L., 2017. Late Quaternary environmental dynamics in the Atacama Desert reconstructed from rodent midden pollen records. J. Quat. Sci. 32 (6), 665–684.

Díaz, F.P., Latorre, C., Carrasco-Puga, G., Wood, J.R., Wilmshurst, J.M., Soto, D.C., Cole, T.L., Gutiérrez, R.A., 2019. Multiscale climate change impacts on plant diversity in the Atacama Desert. Global Change Biol. 25, 1733–1745.

Erfanian, A., Wang, G., Fomenko, L., 2017. Unprecedented drought over tropical South America in 2016: significantly under-predicted by tropical SST. Sci. Rep. 7, 5811.

Faegri, K., Iversen, J., 1989. Textbook of Pollen Analysis, four ed. Joh Wiley & Sons, New York.

Fornace, K.L., Hughen, K.A., Shanahan, T.M., Fritz, S.C., Baker, P.A., Sylva, S.P., 2014. A 60,000-year record of hydrologic variability in the Central Andes from the hydrogen isotopic composition of leaf waxes in Lake Titicaca sediments. Earth Planet Sci. Lett. 408, 263–271.

Garreaud, R.D., Vuille, M., Compagnucci, R., Marengo, J., 2009. Present-day south American climate. Palaeogeogr. Palaeoclimatol. Palaeoecol. 281, 180–195.

Gayo, E.M., Latorre, C., Santoro, C.M., Maldonado, A., De Pol-Holz, R., 2012. Hydroclimate variability in the low-elevation Atacama Desert over the last 2500 yr. Clim. Past 8, 287–306.

Gayo, E.M., McRostie, V.B., Campbell, R., Flores, C., Maldonado, A., Uribe-Rodriguez, M., Moreno, P.I., Santoro, C.M., Christie, D.A., Muñoz, A.A., 2019. Geohistorical records of the anthropocene in Chile. Elem Sci Anth 7.

Giralt, S., Moreno, A., Bao, R., Sáez, A., Prego, R., Valero-Garcés, B.L., Pueyo, J.J., González-Sampériz, P., Taberner, C., 2008. A statistical approach to disentangle environmental forcings in a lacustrine record: the Lago Chungará case (Chilean Altiplano). J. Paleolimnol. 40, 195–215.

Grimm, A.M., 2019. South American Monsoon and its Extremes, Tropical Extremes. Elsevier, pp. 51–93.

Grimm, E.C., 1987. CONISS: a FORTRAN 77 program for stratigraphically constrained cluster analysis by the method of incremental sum of squares. Comput. Geosci. 13, 13–35.

Grosjean, M., Van Leeuwen, J., Van Der Knaap, W., Geyh, M., Ammann, B., Tanner, W., Messerli, B., Núñez, L., Valero-Garcés, B., Veit, H., 2001. A 22,000 14 C year BP sediment and pollen record of climate change from Laguna Miscanti (23 S), northern Chile. Global Planet. Change 28, 35–51.

Han, T., Yu, K., Yan, H., Yan, H., Tao, S., Zhang, H., Wang, S., Chen, T., 2019. The decadal variability of the Global Monsoon links to the North Atlantic climate since 1851. Geophys. Res. Lett. 46, 9054–9063.

Haug, G.H., Hughen, K.A., Sigman, D.M., Peterson, L.C., Röhl, U., 2001. Southward migration of the intertropical convergence zone through the Holocene. Science 293, 1304–1308.

Heiri, O., Lotter, A.F., Lemcke, G., 2001. Loss on ignition as a method for estimating organic and carbonate content in sediments: reproducibility and comparability of results. J. Paleolimnol. 25, 101–110.

Hogg, A.G., Hua, Q., Blackwell, P.G., Niu, M., Buck, C.E., Guilderson, T.P., Heaton, T.J., Palmer, J.G., Reimer, P.J., Reimer, R.W., Turney, C.S.M., Zimmerman, S.R.H., 2013. SHCal13 southern Hemisphere calibration, 0–50,000 Years cal BP. Radiocarbon 55, 1889–1903.

Hooper, J., Marx, S.K., May, J.-H., Lupo, L.C., Kulemeyer, J.J., Pereira, E.d.l.Á., Seki, O., Heijnis, H., Child, D., Gadd, P., 2020. Dust deposition tracks late-Holocene shifts in monsoon activity and the increasing role of human disturbance in the Puna-Altiplano, northwest Argentina. Holocene, 0959683619895814.

Jankovská, V., Komárek, J., 2000. Indicative value of Pediastrum and other coccal green algae in palaeoecology. Folia Geobot. 35, 59–82.

Jara, I.A., Maldonado, A., González, L., Hernández, A., Sáez, A., Giralt, S., Bao, R., Valero Garcés, B.L., 2019. Centennial-scale precipitation anomalies in the southern Altiplano (18° S) suggest an extratropical driver for the South American summer monsoon during the late Holocene. Clim. Past 15, 1845–1859.

Jomelli, V., Khodri, M., Favier, V., Brunstein, D., Ledru, M.-P., Wagnon, P., Blard, P.-H., Sicart, J.-E., Braucher, R., Grancher, D., 2011. Irregular tropical glacier retreat over the Holocene epoch driven by progressive warming. Nature 474, 196.

Kanner, L.C., Burns, S.J., Cheng, H., Edwards, R.L., Vuille, M., 2013. High-resolution variability of the South American summer monsoon over the last seven millennia: insights from a speleothem record from the central Peruvian Andes. Quat. Sci. Rev. 75, 1–10.

Kock, S.T., Schittek, K., Mächtle, B., Maldonado, A., Vos, H., Lupo, L.C., Kulemeyer, J.J., Wissel, H., Schäbitz, F., Lücke, A., 2020. Multi-centennial-scale variations of South American summer monsoon intensity in the southern central Andes (24-27° S) during the late Holocene. Geophys. Res. Lett. 47 (4), e2019GL084157.

Kock, S.T., Schittek, K., Wissel, H., Vos, H., Ohlendorf, C., Schäbitz, F., Lupo, L.C., Kulemeyer, J.J., Lücke, A., 2019. Stable oxygen isotope records (δ18O) of a high-Andean cushion peatland in NW Argentina (24° S) imply South American Summer Monsoon related moisture changes during the Late Holocene. Front. Earth Sci. 7, 45.

Latorre, C., Betancourt, J.L., Rylander, K.A., Quade, J., 2002. Vegetation invasions into absolute desert: a 45 000 yr rodent midden record from the Calama–Salar de Atacama basins, northern Chile (lat 22°–24° S). Geol. Soc. Am. Bull. 114, 349–366.

Latorre, C., Betancourt, J.L., Rylander, K.A., Quade, J., Matthei, O., 2003. A vegetation history from the arid prepuna of northern Chile (22–23 S) over the last 13 500 years. Palaeogeogr. Palaeoclimatol. Palaeoecol. 194, 223–246.

Lenters, J., Cook, K., 1997. On the origin of the Bolivian high and related circulation features of the South American climate. J. Atmos. Sci. 54, 656–678.

Lenters, J., Cook, K.H., 1999. Summertime precipitation variability over South America: role of the large-scale circulation. Mon. Weather Rev. 127, 409–431.

Maldonado, Betancourt, J.L., Latorre, C., Villagran, C., 2005. Pollen analyses from a 50 000-yr rodent midden series in the southern Atacama Desert (25° 30′ S). J. Quat. Sci. 20, 493–507.

Maldonado, A., Uribe, M., 2012. Paleoambientes y ocupaciones humanas en tarapacá durante el período formativo y comienzos del intermedio tardío. XIX Congreso Nacional de Arqueología Chilena, Arica, Chile.

Markgraf, V., 1980. Pollen dispersal in a mountain area. Grana 19, 127–146.

Matthias, I., Giesecke, T., 2014. Insights into pollen source area, transport and deposition from modern pollen accumulation rates in lake sediments. Quat. Sci. Rev. 87, 12–23.

McKee, C.M., 2001. Volcanology and Petrology of Volcán Mino, Andean Central Volcanic Zone.
Morales, M., Christie, D., Villalba, R., Argollo, J., Pacajes, J., Silva, J., Alvarez, C., Llancabure, J., Gamboa, C.S., 2012. Precipitation changes in the South American Altiplano since 1300 AD reconstructed by tree-rings. Clim. Past 8, 653.
Mujica, M.I., Latorre, C., Maldonado, A., González-Silvestre, L., Pinto, R., de Pol-Holz, R., Santoro, C.M., 2015. Late Quaternary climate change, relict populations and present-day refugia in the northern Atacama Desert: a case study from Quebrada La Higuera (18° S). J. Biogeogr. 42, 76–88.
Neukom, R., Rohrer, M., Calanca, P., Salzmann, N., Huggel, C., Acuña, D., Christie, D.A., Morales, M.S., 2015. Facing unprecedented drying of the Central Andes? Precipitation variability over the period AD 1000–2100. Environ. Res. Lett. 10, 084017.
Neukom, R., Steiger, N., Gómez-Navarro, J.J., Wang, J., Werner, J.P., 2019. No evidence for globally coherent warm and cold periods over the preindustrial Common Era. Nature 571, 550–554.
Nobre, P., Shukla, J., 1996. Variations of sea surface temperature, wind stress, and rainfall over the tropical Atlantic and South America. J. Clim. 9, 2464–2479.
Novello, V.F., Vuille, M., Cruz, F.W., Stríkis, N.M., De Paula, M.S., Edwards, R.L., Cheng, H., Karmann, I., Jaqueto, P.F., Trindade, R.I., 2016. Centennial-scale solar forcing of the South American Monsoon System recorded in stalagmites. Sci. Rep. 6, 24762.
Pascale, S., Carvalho, L.M.V., Adams, D.K., Castro, C.L., Cavalcanti, I.F.A., 2019. Current and future variations of the monsoons of the americas in a warming climate. Current Climate Change Reports 5, 125–144.
Pueyo, J.J., Sáez, A., Giralt, S., Valero-Garcés, B.L., Moreno, A., Bao, R., Schwalb, A., Herrera, C., Klosowska, B., Taberner, C., 2011. Carbonate and organic matter sedimentation and isotopic signatures in Lake Chungará, Chilean Altiplano, during the last 12.3 kyr. Palaeogeogr. Palaeoclimatol. Palaeoecol. 307, 339–355.
Pugnaire, F.I., Morillo, J.A., Armas, C., Rodríguez-Echeverría, S., Gaxiola, A., 2020. Azorella compacta: survival champions in extreme, high-elevation environments. Ecosphere 11.
Putnam, A.E., Broecker, W.S., 2017. Human-induced changes in the distribution of rainfall. Science advances 3, e1600871.
R Core Team, 2014. R: a Language and Environment for Statistical Computing. R Foundation for Statistical Computing.
Rabatel, A., Francou, B., Soruco, A., Gomez, J., Cáceres, B., Ceballos, J.L., Basantes, R., Vuille, M., Sicart, J.E., Huggel, C., Scheel, M., Lejeune, Y., Arnaud, Y., Collet, M., Condom, T., Consoli, G., Favier, V., Jomelli, V., Galarraga, R., Ginot, P., Maisincho, L., Mendoza, J., Ménégoz, M., Ramirez, E., Ribstein, P., Suarez, W., Villacis, M., Wagnon, P., 2013. Current state of glaciers in the tropical Andes: a multi-century perspective on glacier evolution and climate change. Cryosphere 7, 81–102.
Rech, J.A., Quade, J., Hart, W.S., 2003. Isotopic evidence for the source of Ca and S in soil gypsum, anhydrite and calcite in the Atacama Desert, Chile. Geochem. Cosmochim. Acta 67, 575–586.
Reyers, M., Shao, Y., 2019. Cutoff lows off the coast of the Atacama Desert under present day conditions and in the last glacial maximum. Global Planet. Change 181, 102983.
Rodríguez, R., Marticorena, C., Alarcón, D., Baeza, C., Cavieres, L., Finot, V., Fuentes, N., Kiessling, A., Mihoc, M., Pauchard, A., 2018. Catálogo de las plantas vasculares de Chile. Gayana. Botánica 75, 1–430.
Rosa, E.B., Pezzi, L.P., Quadro, M.F.L.D., Brunsell, N., 2020. Automated detection algorithm for SACZ, oceanic SACZ and their climatological features. Frontiers in Environmental Science 8, 18.
Sáez, A., Valero-Garcés, B.L., Moreno, A., Bao, R., Pueyo, J., González-Sampériz, P., Giralt, S., Taberner, C., Herrera, C., Gibert, R.O., 2007. Lacustrine sedimentation in active volcanic settings: the Late Quaternary depositional evolution of Lake Chungará (northern Chile). Sedimentology 54, 1191–1222.
Segura, H., Espinoza, J.C., Junquas, C., Takahashi, K., 2016. Evidencing decadal and interdecadal hydroclimatic variability over the Central Andes. Environ. Res. Lett. 11, 094016.
Seltzer, G., Rodbell, D., Burns, S., 2000. Isotopic evidence for late Quaternary climatic change in tropical South America. Geology 28, 35–38.
Stríkis, N.M., Cruz, F.W., Cheng, H., Karmann, I., Edwards, R.L., Vuille, M., Wang, X., de Paula, M.S., Novello, V.F., Auler, A.S., 2011. Abrupt variations in South American monsoon rainfall during the Holocene based on a speleothem record from central-eastern Brazil. Geology 39, 1075–1078.
Sulca, J., Takahashi, K., Espinoza, J.C., Vuille, M., Lavado-Casimiro, W., 2018. Impacts of different ENSO flavors and tropical Pacific convection variability (ITCZ, SPCZ) on austral summer rainfall in South America, with a focus on Peru. Int. J. Climatol. 38, 420–435.
Sulca, J., Vuille, M., Silva, Y., Takahashi, K., 2016. Teleconnections between the Peruvian central Andes and northeast Brazil during extreme rainfall events in austral summer. J. Hydrometeorol. 17, 499–515.
Teillier, S., 2004. La vegetación de la cuenca media-alta del río Loa (3100-4150 msnm), Región de Antofagasta (II), Chile. Chloris Chil. 7.
Trivelli, M.Á., Valdivia, V., 2009. Alcances sobre flora y vegetación de la cordillera de los Andes. Región de Arica y Parinacota y Región de Tarapacá.
Tully, C.D., Rech, J.A., Workman, T.R., Santoro, C.M., Capriles, J.M., Gayo, E.M., Latorre, C., 2019. In-stream wetland deposits, megadroughts, and cultural change in the northern Atacama Desert, Chile. Quat. Res. 91, 63–80.
Utida, G., Cruz, F.W., Etourneau, J., Bouloubassi, I., Schefuß, E., Vuille, M., Novello, V.F., Prado, L.F., Sifeddine, A., Klein, V., 2019. Tropical South Atlantic influence on Northeastern Brazil precipitation and ITCZ displacement during the past 2300 years. Sci. Rep. 9, 1–8.
Van Breukelen, M., Vonhof, H., Hellstrom, J., Wester, W., Kroon, D., 2008. Fossil dripwater in stalagmites reveals Holocene temperature and rainfall variation in Amazonia. Earth Planet Sci. Lett. 275, 54–60.
Viale, M., Bianchi, E., Cara, L., Ruiz, L.E., Villalba, R., Pitte, P., Masiokas, M., Rivera, J.A., Zalazar, L., 2019. Contrasting climates at both sides of the Andes in Argentina and Chile. Frontiers in Environmental Science 7, 69.
Viana, J.C.C., Sifeddine, A., Turcq, B., Albuquerque, A.L.S., Moreira, L.S., Gomes, D.F., Cordeiro, R.C., 2014. A late Holocene paleoclimate reconstruction from Boqueirão Lake sediments, northeastern Brazil. Palaeogeogr. Palaeoclimatol. Palaeoecol. 415, 117–126.
Villagrán, C., Armesto, J.J., Kalin Arroyo, M.T., 1981. Vegetation in a high andean transect between turi and Cerro león in northern Chile. Plant Ecol. 48, 3–16.
Villagrán, C., Kalin Arroyo, M.T., Marticorena, C., 1983. Efectos de la desertización en la distribución de la flora andina de Chile. Rev. Chil. Hist. Nat. 56, 137–157.
Viveen, W., Zevallos-Valdivia, L., Sanjurjo-Sanchez, J., 2019. The influence of centennial-scale variations in the South American summer monsoon and base-level fall on Holocene fluvial systems in the Peruvian Andes. Global Planet. Change 176, 1–22.
Vuille, M., 1999. Atmospheric circulation over the Bolivian Altiplano during dry and wet periods and extreme phases of the Southern Oscillation. Int. J. Climatol. 19, 1579–1600.
Vuille, M., Ammann, C., 1997. Regional snowfall patterns in the high, arid Andes. Climatic Change 36, 413–423.
Vuille, M., Burns, S., Taylor, B., Cruz, F., Bird, B., Abbott, M., Kanner, L., Cheng, H., Novello, V., 2012. A review of the South American monsoon history as recorded in stable isotopic proxies over the past two millennia. Clim. Past 8, 1309–1321.
Vuille, M., Keimig, F., 2004. Interannual variability of summertime convective cloudiness and precipitation in the central Andes derived from ISCCP-B3 data. J. Clim. 17, 3334–3348.
Whitney, B.S., Mayle, F.E., 2012. Pediastrum species as potential indicators of lake-level change in tropical South America. J. Paleolimnol. 47, 601–615.
Zhou, J., Lau, K., 1998. Does a monsoon climate exist over South America? J. Clim. 11, 1020–1040.